Efficient Modal Design Variables for Optimization of Aero-Elastic Wing

D.J. Poole *, C.B. Allen †, T.C.S. Rendall‡

Department of Aerospace Engineering, University of Bristol, Bristol, BS8 1TR, U.K.

Efficient multi-disciplinary optimization is presented for aero-structural wing optimization using efficient low-dimensional modal design variables. Orthogonal aerofoil design variables are derived in the geometric space via singular value decomposition. Orthogonality of design variables leads to a well-conditioned design space and encourages positive optimizer convergence. These are applied in a sectional fashion for fixed planform drag minimization of a flexible transonic wing. Shock-free solutions are demonstrated for the rigid wing, indicating suitability of the aerofoil modes for sectional-based wing optimization. However, these wings have poor performance when deformed under flight loads, hence full aeroelastic performance is taken into account. Encouragingly, shock-free solutions are again found. Loading is shifted outboard, leading to increased tip-deflection. Monotonic improvement in objective with increase in dimensionality is also observed.

I. Introduction

The design of an aircraft is inherently an exercise in the coupling and subsequent compromise of multiple, and often independently considered, disciplines. Nowhere is this more apparent than in the design of aircraft wings, where the aerodynamic performance typically dominates, but where the design is dictated by the behaviour of many other disciplines. Multi-disciplinary optimization (MDO)[1] is the framework that proceeds when analysis of each discipline is integrated into an overall coupled system within an overall optimization framework. In MDO, numerical analysis is used to determine various metrics (or cost functions) to optimize, and constraint functions to make designs realistic. An optimization algorithm is then required to link the analysis to the design process, where the algorithm uses values of the cost and constraints to determine a vector of design variables that link to changes in the design to hopefully improve the cost. A parameterization is the vehicle that governs how the design variables affect the design. An example single-discipline problem is finding the optimum geometry of aerofoils or wings to minimise drag subject to a constraint on lift, where a computational fluid dynamics (CFD) solver is used to determine the aerodynamic performance; see[2–6] for example.

In aircraft wing design, the aero-structural coupled system dominates the performance. Simulation of this system either requires coupling of separate CFD and computational structural mechanics (CSM) solvers in a partitioned manner,[7–9] or developing one overall solver in a monolithic manner.[10,11] While accuracy and convergence tends to be better with the monolithic approach, the development costs are a barrier. For example, all four codes that submitted results to the aero-structural benchmarking case of the Sixth AIAA CFD Drag Prediction Workshop used a partitioned solution approach.[12] For either system, interpolation of forces and moments between the models, and subsequent mesh deformation around the deformed structure are then required. An outer iteration loop is added to march the solution to equilibrium. The interpolation and mesh deformation are often handled separately, but a unified approach using radial basis function (RBF) interpolation was shown to be highly effective.[13] A similar approach, but using B-spline-based methods, has also recently been presented.[14] Once a suitable aero-structural solver is developed, full MDO of the wing that optimizes for the performance of the coupled aerodynamic and structural responses can be realised, see[15] for example. Local gradient-based optimization algorithms have usually been the tool of choice for these types

*Lecturer in Aerodynamics. Email: d.j.poole@bristol.ac.uk

†Professor of Computational Aerodynamics. AIAA Senior Member. Email: c.b.allen@bristol.ac.uk

‡Senior Lecturer in Aerodynamics. AIAA Member. Email: thomas.rendall@bristol.ac.uk

of optimization problem. Cost and constraint gradients can be evaluated using the adjoint approach,[16] for example.[17,18] Furthermore, recent developments include the ongoing work to couple more disciplines into the process, including coupling aerodynamics, structures and acoustics in a fully coupled unsteady optimization of rotorcraft.[19]

Large numbers of design variables permit detailed small-scale optimization. However, the quantity of design variables has a significant effect on the convergence of the optimizer. Furthermore, while gradient-based methods are popular optimization algorithms in MDO, if alternatives (such as population-based) methods are to be exploited, then lower-dimensional design spaces become key. Hence, dimensionality reduction techniques have become a useful approach for reducing the dimensionality associated with aerodynamic shape optimization. Of these, singular value decomposition-based approaches take a training matrix of data (for example a number of aerofoil shapes[20,21]), and project a reduced-order basis approximation of the original data. Work by the authors has shown that this is a very efficient approach for filtering the design space and producing a reduced, orthogonal set of aerofoil deformation modes.[22] Orthogonality is key to encourage good optimizer convergence by providing a well-conditioned design space, with minimal coupling between design variables. These are applicable to aerodynamic optimization of aerofoils[5] and wings.[23] Furthermore, comprehensive experiments[24] have shown singular value decomposition (SVD) modes to be the most efficient approach at representing a generic aerofoil compared to most other commonly used parameterization methods.

The work presented in this paper extends the application of these modes further by considering high-fidelity aero-structural wing optimization. In a previous publication by the authors at SciTech 2019,[25] a preliminary proof-of-concept study was presented that applied the compact aerofoil deformation modes to aerodynamic shape optimization of a wing in jig-shape and flight-shape. The work in this paper builds on that study by applying the design variables for aerodynamic shape optimization within a fully coupled solver. In addition, dimensionality of the design space is studied.

The remainder of the paper is organised as follows: the compact modal decomposition and how this is applied to wing optimization is outlined in section II; the solver and datum solution is presented in section III; the optimization problem and chosen optimizer is presented in section IV; optimization of the rigid wing and aeroelastic wing are presented in sectionsV and VI, respectively; finally, conclusions are given in section VII.

II. Decomposition for Wing Design Variables

The design variables used in the optimization process are the weightings of various sectional deformations. These sectional deformations come about by performing a matrix decomposition that uses SVD on a training library of aerofoils. The resulting modes represent a reduced basis projection of the full-basis aerofoil design space. The modes are also orthogonal, which leads to a well conditioned design space, and no coupling of variables in the geometric space. This aids optimizer convergence considerably. Full wing deformations are separable into sectional and planform deformations, which is also performed here. The aerofoil deformation modes from the SVD are applied sectionally, then planform deformations are applied. The full process of obtaining and applying these deformations are described below.

II.A. SVD for Sectional Deformations

To obtain aerofoil deformation modes, a training library of aerofoils needs to first be collated. The selection of the training library is one of the most important steps in this process since the characteristics of the library map to the characteristics of the deformation modes. The authors have previously published work[22] that used a metric-based filtering approach to select the training library. In this work, the library of aerofoils is as previously used by the authors for transonic aerofoil optimization.[5] The aerofoil data was obtained from the UIUC database[a], and was subsequently smoothed and re-parameterised to ensure consistency.

A training library contains M aerofoils each parameterised with N surface points, where the i-th surface point of the m-th aerofoil has coordinates (x_{i_m}, z_{i_m}). To obtain aerofoil deformation modes, the vector difference between each surface point of all aerofoils is computed. The vector difference of the i-th surface point between the m-th and n-th aerofoils is given as $(\Delta x_{i_{m,n}}, \Delta z_{i_{m,n}})$,.

[a] http://m-selig.ae.illinois.edu/ads/coord_database.html

All deformations are collated into a single deformation matrix that has $2N$ rows and $M_{def} = M(M-1)/2$ columns:

$$\mathbf{\Psi} = \begin{pmatrix} \Delta x_{1_{1,2}} & \cdots & \Delta x_{1_{1,M}} & \Delta x_{1_{2,3}} & \cdots & \Delta x_{1_{M-1,M}} \\ \vdots & \ddots & \vdots & \vdots & \ddots & \vdots \\ \Delta x_{N_{1,2}} & \cdots & \Delta x_{N_{1,M}} & \Delta x_{N_{2,M}} & \cdots & \Delta x_{N_{M-1,M}} \\ \Delta z_{1_{1,2}} & \cdots & \Delta z_{1_{1,M}} & \Delta z_{1_{2,3}} & \cdots & \Delta z_{1_{M-1,M}} \\ \vdots & \ddots & \vdots & \vdots & \ddots & \vdots \\ \Delta z_{N_{1,2}} & \cdots & \Delta z_{1_{1,M}} & \Delta z_{N_{2,M}} & \cdots & \Delta z_{N_{M-1,M}} \end{pmatrix}$$

The deformation matrix has an SVD given by:

$$\mathbf{\Psi} = \mathbf{U}\mathbf{\Sigma}\mathbf{V}^T \tag{1}$$

where $\mathbf{U}$ is an orthonormal $2N \times 2N$ matrix, $\mathbf{\Sigma}$ is a diagonal matrix with $\min\{2N, M_{def}\}$ diagonal entries arranged in descending order, and $\mathbf{V}^T$ is an orthonormal $M_{def} \times M_{def}$ matrix. The columns of $\mathbf{U}$ contain the aerofoil deformation modes, and these are extracted column-wise and used for the optimization. The diagonal entries of $\mathbf{\Sigma}$ contain the singular values, which may be used to determine now much 'energy' each mode has in the overall system.

The use of the SVD here is for geometric filtration of the high-degree training matrix into a low-degree representation using deformation modes. To do this, the first D modes (i.e. first D columns of U) may be extracted and a D-rank approximation of the original matrix may be obtained by:

$$\mathbf{\Psi} \approx \mathbf{\Psi}^{(D)} = \widetilde{\mathbf{U}}\widetilde{\mathbf{\Sigma}}\widetilde{\mathbf{V}}^T \tag{2}$$

where the tilde is used to denote reduced forms of the SVD matrices. Once a low-rank approximation is found through SVD, the following is true:[26]

$$\|\mathbf{\Psi} - \mathbf{\Psi}^{(D)}\|_F \leq \|\mathbf{\Psi} - \mathbf{\Phi}\|_F \tag{3}$$

where $\mathbf{\Phi}$ is any matrix of rank D and $\|\cdot\|_F$ is the Frobenius norm. Hence, the error between the low-rank approximation and the full rank approximation will always be at least as good as the error between any other k-rank matrix and the full-rank matrix. In this sense, the SVD produces an optimal low order projection of the higher dimensional space into the lower dimensional one.

The first four deformation modes are shown in figure 1 (these are superimposed on NACA0012 for visualisation purposes). It is clear to see that the first mode represents a thickness change, then the second represents a camber change, indicating that for this library of aerofoils, these are the two most important aerofoil design parameters respectively.

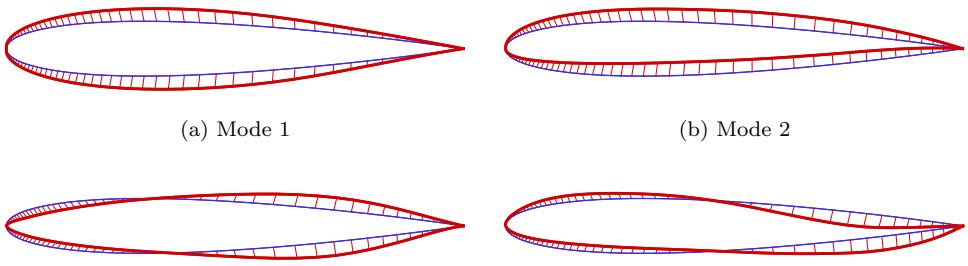

(a) Mode 1

(b) Mode 2

(c) Mode 3

(d) Mode 4

Figure 1: First four aerofoil deformation modes (superimposed on NACA0012 for visualisation)

Given the required number of deformation modes, D, in the optimization, the design variables are the weightings of each deformation mode. The overall deformation is then a linear superposition of each mode:

$$\mathbf{\Delta X} = \sum_{i=1}^{D} \alpha_i \mathbf{U}_i \tag{4}$$

where α_i is the design variable relating to the i-th mode and $\mathbf{U}_i$ is the i-th mode, which is the i-th column of $\mathbf{U}$.

II.B. Application to Wing Deformation

The aerofoil deformation modes are surface deformations, however, to ensure body-fitted meshes are retained in the optimization the mesh also needs to deform. Furthermore, the surface deformation modes are applied sectionally, which is defined here.

The sectional deformations are applied at a fixed number of spanwise stations, i.e. equation 4 is applied at these stations locally. However, the sectional deformations can also be applied in a global nature, and while this is not as flexible as local deformation, the authors have shown global deformations to provide reasonable optimization results but at a fraction of the cost.[23] The sectional deformations are applied using the RBF control point approach, where a set of control points are defined in the fluid domain and global volume interpolation translates deformation of the control points to deformation of the aerodynamic mesh. Hence, the modal deformations are used to drive deformation of the control points that subsequently deform the wing surface and mesh. These deformations are decoupled, so the control point modal deformations are determined off-line and then applied in the optimization process.

At the heart of this technique in an RBF interpolation developed originally for aero-structure coupling and mesh motion by Rendall and Allen.[13] An RBF interpolation, s, is a linear combination of basis functions, whose argument is the Euclidean distance, $\|\cdot\|$ between the point to be interpolated in the domain, $\mathbf{x}$, and the N points in the known data set. Therefore, the influence that a known point has is controlled by a function, ϕ, that depends on the distance from the interpolated point:

$$s(\mathbf{x}) = \sum_{i=1}^{N} \beta_i \phi(\|\mathbf{x} - \mathbf{x}_i\|) + p(\mathbf{x}) \tag{5}$$

Control points decouple the shape deformations from the surface mesh and provide a unified framework for surface and mesh deformation. Given n_c control points, a global RBF interpolation of this nature provides exact recovery of data at known sites, and interpolation of that data away from the sites. In the case of optimization, the data to be interpolated is deformation of the control points, hence a deformation field is created. The position of the aerodynamic mesh points in the field therefore defines the deformation of those points. Since exact recovery of data at the know sites (in this case the position of the control points, which for the j-th control point is defined as $(x_{c_j}, y_{c_j}, z_{c_j})$) is specified, the interpolation takes the form:

$$\Delta\mathbf{x}_c = \mathbf{M}\boldsymbol{\beta}^x$$

where

$$\Delta\mathbf{x}_c = \begin{pmatrix} \Delta x_{c_1} \\ \vdots \\ \Delta x_{c_{n_c}} \end{pmatrix} \qquad \boldsymbol{\beta}^x = \begin{pmatrix} \beta_1^x \\ \vdots \\ \beta_{n_c}^x \end{pmatrix} \qquad \mathbf{M} = \begin{pmatrix} \phi_{1,1} & \cdots & \phi_{1,n_c} \\ \vdots & \ddots & \vdots \\ \phi_{n_c,1} & \cdots & \phi_{n_c,n_c} \end{pmatrix}$$

and analogous definitions hold for the y and z coordinates. The radial basis function $\phi_{i,j} = \phi(\|\mathbf{x}_{c_i} - \mathbf{x}_{c_j}\|)$ can take a number of forms, but the radially-decaying functions of Wendland[27] are a good choice for the mesh deformation problem to give the interpolation a local character and ensure deformation is contained in a region near the moving body. The C^2 function is used here.

Once the linear system is solved, the resulting deformation field can be evaluated at the location of each mesh point. The deformation of an aerodynamic mesh point is given by:

$$\Delta x_a = \sum_{i=1}^{n_c} \beta_i^x \phi(\|\mathbf{x}_{c_i} - \mathbf{x}_a\|) \tag{6}$$

with analogous definitions for y and z.

Using RBF interpolation has the advantage of being able to specify the level of control since control points can be placed arbitrarily in, on the boundary, or outside the fluid domain. However, irrespective of

the location of the control points, modal deformations defined on the aerofoil surface may not be coincident with the control points so control point deformations must be defined. The authors[28] showed a number of techniques for achieving this, and an inverse RBF interpolation is an effective approach. The set-up of control points around the wing used in this paper is shown in figure 2.

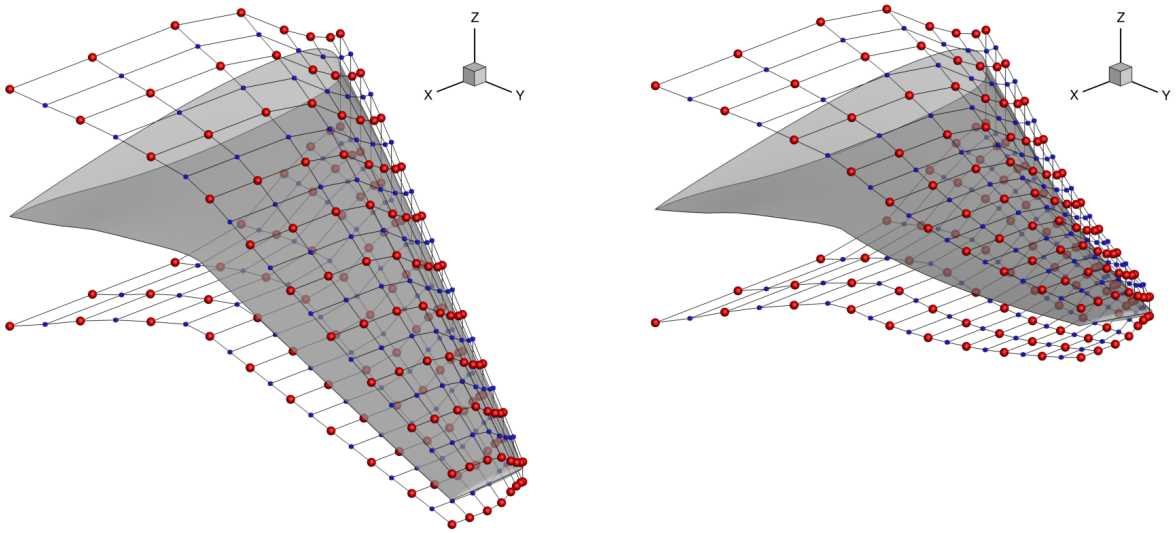

Figure 2: Control point cages around rigid and aeroelastic wing

Modal deformations are applied sectionally at ten spanwise station (on the red main control points), while intermediate control points (shown in blue) are used to permit smooth spanwise deformations between the deformation slices.[23] The deformation of intermediate points uses a partition of unity-blend of the deformation slices at either side. To define deformations of a slice of intermediate control points, Δ_i, then the deformations of the slices of main control points on either side of the intermediate slice (Δ_m and Δ_{m+1}) are blended as:

$$\Delta_i = \Delta_m \cos^2\left(\frac{\pi\lambda}{2}\right) + \Delta_{m+1} \sin^2\left(\frac{\pi\lambda}{2}\right)$$

where $\lambda = (y_i - y_m)/(y_{m+1} - y_m)$. Hence, it can be seen that if the main deformations are equivalent of two neighbouring sections ($\Delta_m = \Delta_{m+1}$) then any intermediate slice will have the same deformation.

In addition to the sectional deformations, a global twist deformation is introduced. A linear twist is applied from zero at the root to the twist angle at the tip. Hence, the local angle of rotation, γ, of a main control point slice located at y_m is given by $\gamma(y_m) = \gamma y_m/s$.

The control point cage is constructed around the local wing coordinates. For example, figure 2 shows the cage around both a rigid wing and a deformed wing. Hence, the sequence of operations is given a design variable vector, $\boldsymbol{\alpha}$, twist deformations of the main sections occurs, followed by sectional deformations at main spanwise stations. The intermediate sectional deformations are then calculated. Once all control point deformations are defined and calculated, mesh deformation occurs.

III. Aero-structural Solver and Case Definition

For optimization, it is important that changes in objectives, constraints and gradients are accurately captured. This is particularly important if, like in this paper, gradients are evaluated using finite difference where small perturbations to the design variables are used to approximate the gradient value; if the resulting objective function evaluations are not of sufficient resolution then gradient values can be wildly incorrect leading to poor optimizer performance, or worse, an ill-posed problem. Here, this requires having a solver and a mesh that minimises any numerical noise or spurious drag.

The aero-structural solver is based on the structured multiblock solver of Allen,[29,30] with the coupled solver added through the work of Rendall and Allen.[13] In the case considered in this work, the flow is governed

by the Euler equations, which are solved using finite volume integration with the Jameson-Schmidt-Turkel scheme.[31] Convergence acceleration is achieved through multigrid.[32] A modal structural solver is applied where coupling between the aerodynamic and structural grids, and subsequent mesh motion, is achieved through RBF coupling[13] that uses a reduced point cloud between aerodynamic and structural neighbour nodes.[33] Strong coupling of the two systems is employed for dynamic calculations. Newmark temporal integration[34] is used to march the solution.

To demonstrate using the compact aerofoil decomposition for aero-structural optimization, the MDO wing[35,36] is used, where the structural model and associated structural mode shapes are defined. Figure 3 shows the MDO wing planform. Also shown is the aerodynamic surface mesh and the structural grid. A 2515 node wing-box structural model is used with the modes defined by Haase *et al.*[36]

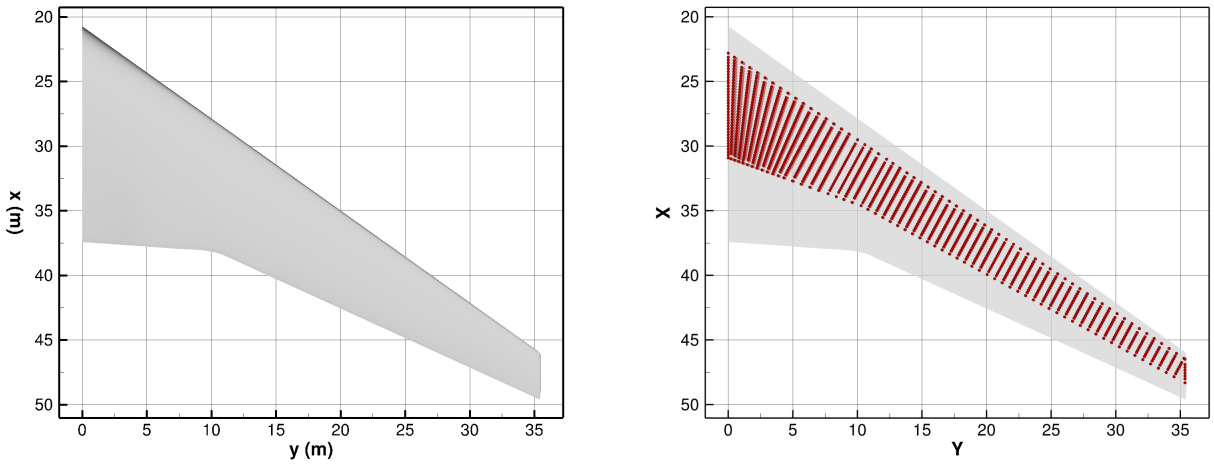

Figure 3: MDO wing and structural mesh in planform view

Throughout this work, a trimmed cruise condition of $C_L = 0.4$ at $M_\infty = 0.85$ is used. Unless otherwise stated, all wings are trimmed to this condition. The MDO wing has 18 defined structural modes and all are used for this work.

To ensure sufficient aerodynamic resolution, a mesh dependence study is presented. A family of eight-block structured C-meshes (block structure is given in figure 4) was generated using the methods of Allen[37] to give high quality meshes. These range in size from 2.1 million to 0.13 million cells, and are designated L1 (2.1mil), L2 (1.1mil), L3 (580k), L4 (260k) and L5 (130k); sizes were chosen with approximately a two-times scaling between mesh levels, and to maximise the number of multigrid levels for each mesh.

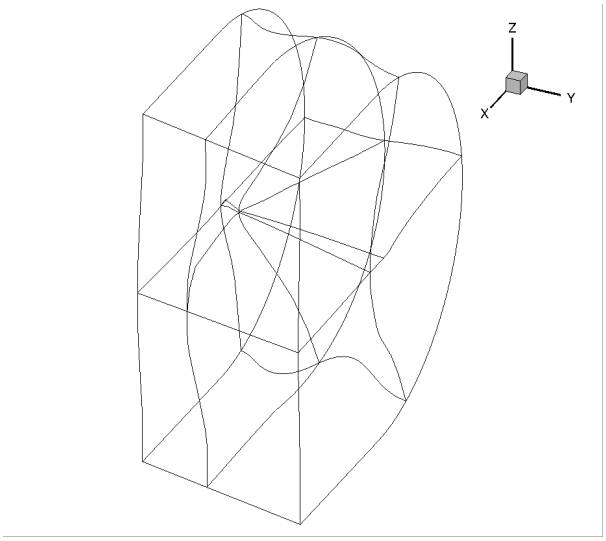

Figure 4: Block structure of eight-block structured C-meshes

Each mesh was used to produce both a static and aeroelastic solution and the final force coefficients of each run are given in table 1. The structural deflection is calculated based on the deformation of the structural node closest to the aerodynamic tip. Also given are the run-times relative to the run-time of the coarsest mesh, with the runs being performed in serial to obtain comparable figures. All wings were run at a trimmed cruise C_L of 0.4. Figure 5 gives the surface pressure coefficients of the coarsest and finest meshes. Clearly, there is little difference in the flowfields, but the finer meshes capture the shock more sharply. The L4 mesh, while being relatively coarse, appears to be a good compromise between run-time and accuracy.

Table 1: Force coefficients and run-times (relative to L5 mesh) on different meshes

	Static			Aeroelastic			
Mesh	C_L	C_D	Run-time (×L5)	C_L	C_D	Δz_{struc}	Run-time (×L5)
L5	0.4	0.0192	1.0	0.4	0.0211	6.15m	1.0
L4	0.4	0.0158	2.2	0.4	0.0177	6.18m	1.7
L3	0.4	0.0134	4.9	0.4	0.0153	6.19m	3.9
L2	0.4	0.0121	7.2	0.4	0.0137	6.10m	7.4
L1	0.4	0.0119	11.9	0.4	0.0134	6.12m	11.8

The primary mesh used for the study is the L4 mesh, shown in figure 6, which contains 273k nodes. This mesh has a 97×57 surface mesh, 21 nodes on either side of the wake, and 25 nodes between the inner and outer boundary.

Figure 7 shows the solution of the static MDO wing and the aeroelastic wing (i.e. in flight shape). and figure 8 gives the span-wise loading distribution. There is a strong stock present on the static wing, that when in flight-shape is no longer present outboard. The loading is shifted inboard and the distribution is almost perfectly triangular in flight shape. This results in a lower root bending moment at the expense of a drag penalty.

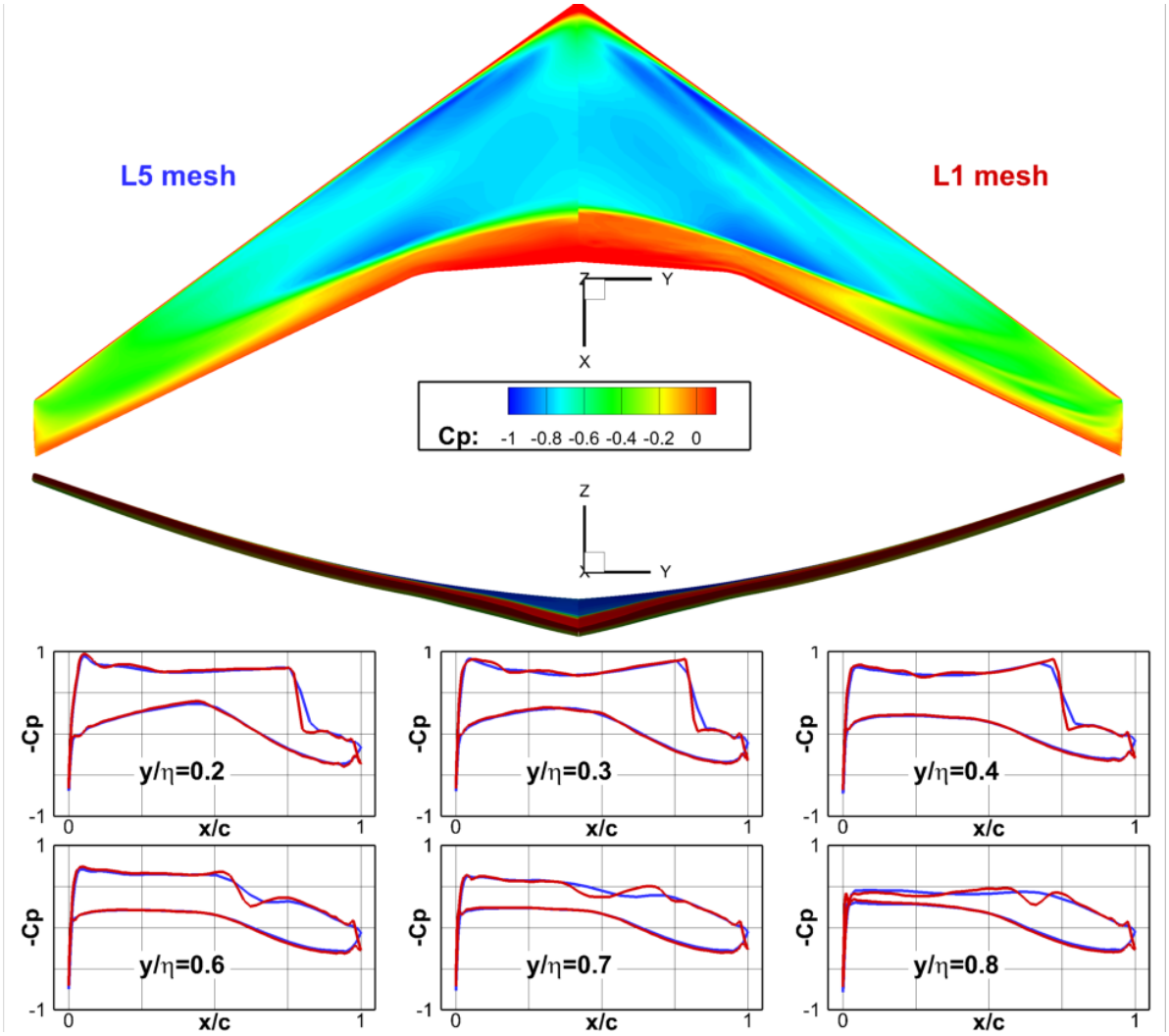

Figure 5: Surface C_P of aeroelastic wing shape on L5 and L1 meshes

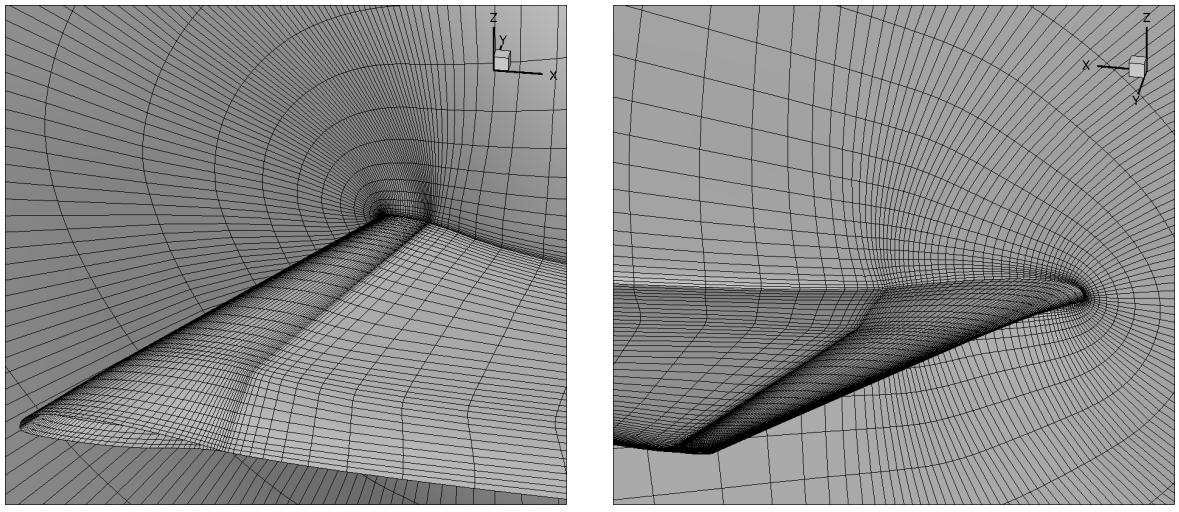

Figure 6: L4 mesh

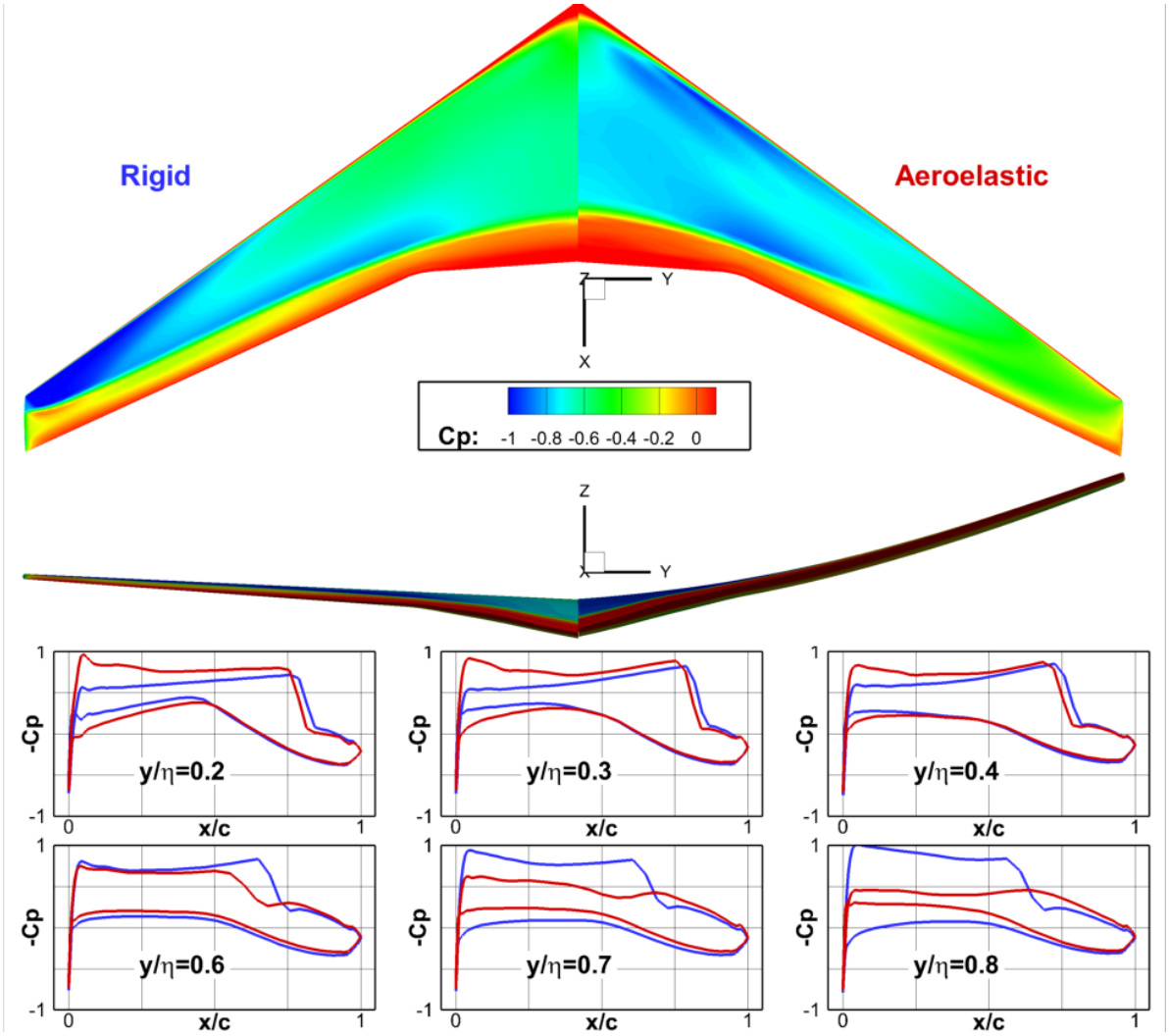

Figure 7: Surface C_P of rigid and aeroelastic wing shapes on optimisation mesh (L4)

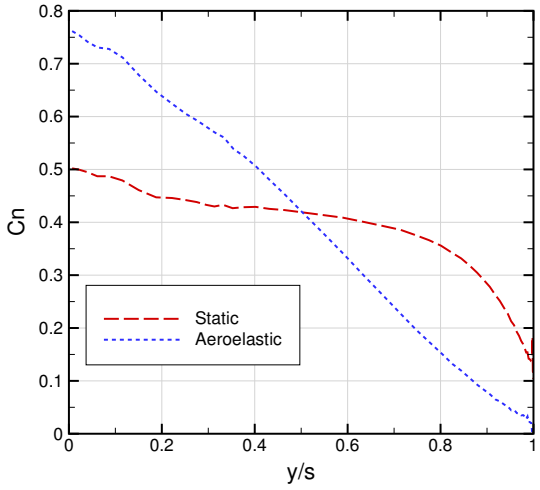

Figure 8: Span-wise loading on MDO wing

IV. Optimization Problem and Algorithm

A generic single-objective optimization problem optimizes a cost function, J, which is a function of a vector of D design variables, $\boldsymbol{\alpha}$, subject to a vector of inequality constraints, $\mathbf{g}$, and equality, $\mathbf{h}$, constraints. The problem considered in this paper is aerodynamic shape optimization. The objective is drag minimization subject to constraints on lift coefficient, C_L and internal volume V. Further to this, moments have not been considered as constraints to permit full flexibility of the optimizer. Moments are reported throughout for interest. The problem is given by:

$$\begin{aligned} \underset{\boldsymbol{\alpha}\in\Re^D}{\text{minimise}} \quad & C_D \\ \text{subject to} \quad & C_L \geq 0.4 \\ & V \geq V(\text{initial}) \end{aligned} \tag{7}$$

The design variables of the problem are aerofoil deformation modes applied at ten equally spaced sections across the span of the wing. Furthermore, to allow induced drag to reduce, the linear (root-to-tip) twist variable is used, and to allow balance of the lift loading, angle of attack is also a design variable. Details of the different design variables are given in table 2.

Table 2: Numbers of design variables

Global	Local	Total
2 (twist, angle)	40 (4 modes/section × 10 sections)	42
2 (twist, angle)	60 (6 modes/section × 10 sections)	62
2 (twist, angle)	80 (8 modes/section × 10 sections)	82

Using structural modal analysis is an effective means to determine the coupled aero-structural performance of the wing. However, when used in an optimization process, the primary assumption is that modifying the aerodynamic shape has minimal effect on the structural response so the same structural modes can be used. This assumption holds assuming the structure is not changed, and since a wing-box is modelled, no planform changes occur but only minor surface changes, this is reasonable.

In the case considered in this paper, the overall goal of this work is to permit large-scale global aeroelastic shape optimization. Global optimization is particularly useful when the design space is known to be multimodal, and the overall goal is to locate the globally optimal solution. In the first instance, only sectional changes are considered and since fixed planform wing optimization is generally considered to be unimodal (to within numerical tolerances),[38] the gradient-based optimization algorithm, feasible sequential quadratic programming (FSQP) algorithm as implemented in version 3.7,[39] is used. FSQP is based on the sequential quadratic programming (SQP) approach, but modified to improve convergence by combining a search along an arc[40] with a non-monotone procedure for that search.[41] The FSQP algorithm is fully described and analysed in.[42,43]

The gradient-based optimizer requires the sensitivities of the cost and constraint functions with respect to each design variable at each major iteration. For this work, a second-order finite difference stencil is used so for each design variable, two extra flow solutions are required (one each for the positive and negative perturbations) to evaluate the sensitivities. For computational efficiency, a parallel decomposition of the gradient evaluation is employed such that each design design variable sensitivity is assigned to its own CPU, which handles the geometry (and CFD volume mesh) deformations and flow solutions. Once the gradients are evaluated, these are passed back to the master process where the optimizer update occurs. The overall optimization process is similar to that presented by Morris *et al.*[44]

V. Rigid Wing Optimization Results

Initially, to determine both the optimization set-up and a suitable number of SVD modal design variables, optimization of the rigid MDO wing is performed at the trimmed cruise flight condition ($C_L = 0.4$ at $M_\infty = 0.85$).

Table 3 gives the optimization results of the optimizations, while figure 9 gives the convergence of the optimizer. For all three of the design variable combinations tested, both constraints are active and the drag has reduced substantially. Of particular interest is the monotonic decrease in the acquired objective function with increasing number of design variables. In the geometric space, the modal design variables are perfectly orthogonal, which has the implication that the design space of lower numbers of design variables is contained within the design space of higher numbers. In the aerodynamic space, this is not necessarily the case; though the authors have shown this to be the case for aerofoil optimization.[5] Albeit, the monotonic decrease indicates that geometrically orthogonal aerofoil design variables exhibit similar performance when applied to wing optimization.

Table 3: Optimization results of rigid MDO wing

	C_L	C_D	C_{M_x}	C_{M_y}	$V(\mathrm{m}^2)$	ΔC_D
Initial	0.4	0.0158	0.183	-0.476	241.0	-
42 variables	0.4	0.0127	0.172	-0.451	241.0	**-19.6%**
62 variables	0.4	0.0125	0.173	-0.457	241.0	**-20.8%**
82 variables	0.4	0.0124	0.173	-0.457	241.0	**-21.5%**

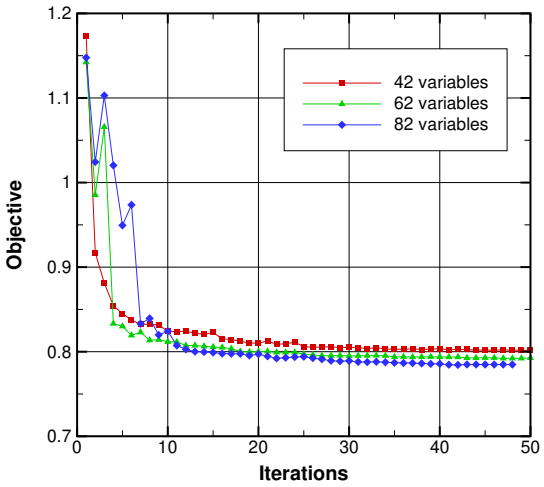

Figure 9: Optimizer convergence for rigid MDO wing

Figure 10 shows the surface pressures of the baseline wing and 8-modes optimized wing, and demonstrates that the result is shock-free at the design condition. Since this problem is inviscid, the two primary sources of drag are wave drag and induced drag. As the problem is shock-free, wave drag has been substantially reduced.

The static rigid optimizations have produced the expected shock-free result at the design condition, however, it is interesting to see how this wing performs under aeroelastic loading. Hence, the optimized wing is run with the structural model to determine the aeroelastic solution. Table 4 gives the force coefficients of the aeroelastic MDO wing and the aeroelastic solution of the optimized rigid wing, while figure 11 shows the surface pressure coefficients. It should be noted that all wings are trimmed to $C_L = 0.4$. Clearly the aeroelastic solution of the optimized rigid wing has a shock structure, with a single shock at the inboard and outboard sections, and a double shock midspan and this has resulted in an overall drag increase. Also, the extra outboard load of the rigid optimised wing has resulted in a lower tip deflection.

It is well known that single-point drag minimization produces highly optimised point-design solutions with poor off-design performance,[45] so an increase in drag for the aeroelastic solution of a rigid wing is not surprising. The changes in loading that occur due to shape changes in optimization, lead to a change in the deflected shape which leads to a further change in the loading. It is therefore not enough to consider

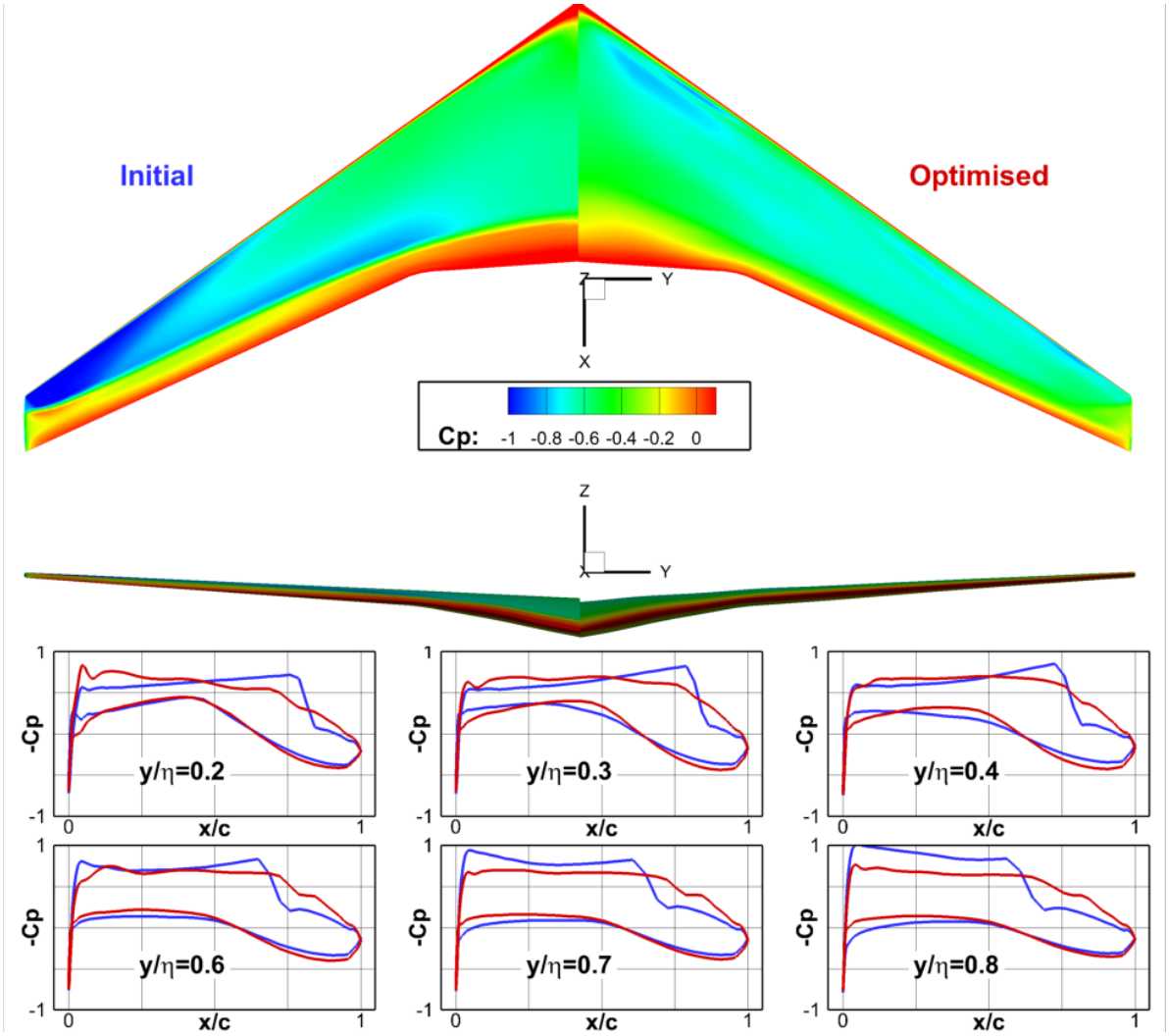

Figure 10: Surface C_P of initial and optimised wing shapes for 8 modes case

Table 4: Forces of aeroelastic MDO wing and aeroelastic solution of optimised rigid wing

	C_L	C_D	C_{M_x}	C_{M_y}	Δz_{struc}(m)
MDO	0.4	0.0177	0.143	-0.382	6.18
Optimised	0.4	0.0203	0.138	-0.375	5.33

optimising a wing statically, but that the full aero-structural solution must be taken into account to obtain any meaningful results.

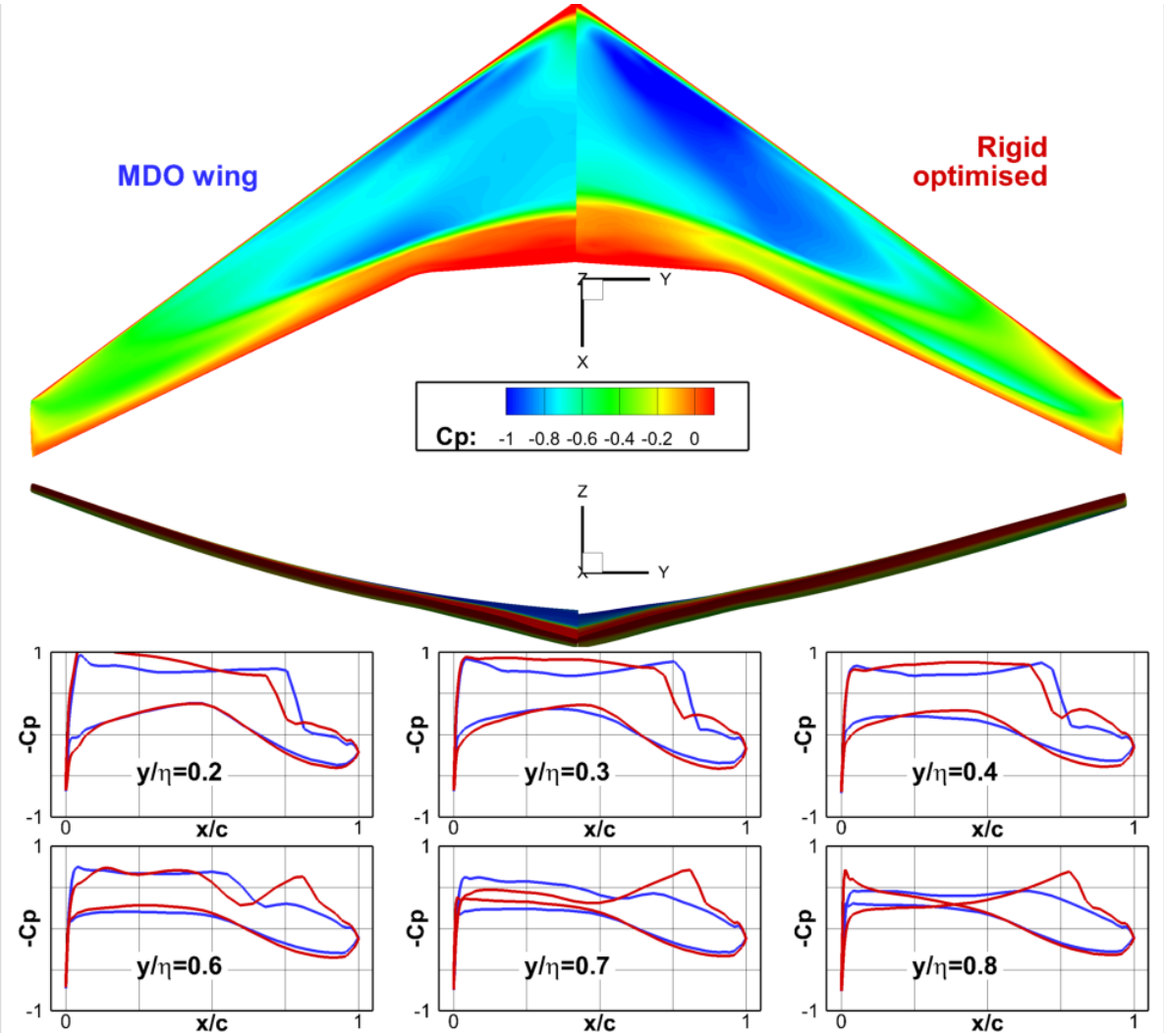

Figure 11: Surface C_P of MDO wing and case I result under aeroelastic loading

VI. Aeroelastic Wing Optimization Results

As a result of the experiment presented above, it is proposed that wing optimizations should contain wing shape responses also. In that light, aerodynamic shape optimizations are presented of the aeroelastic MDO wing.

Table 5 shows the optimization results for varying numbers of modes, and figure 12 gives the optimizer convergence. As in the rigid case, monotonic decrease in the objective function is observed, which is to be expected with the modal design variables, but is encouraging to observe. Both the lift and volume constraints are active for all the cases. The tip deflection has increased substantially for the optimized wing indicating that transferring load from root to tip (the load is almost perfectly triangular in the MDO wing, but close to elliptical in the optimised wing) and allowing a more flexible solution (something observed in modern transonic aircraft) permits shock strength reduction. This is demonstrated in the surface pressure shown in figure 13. Comparison of the wing shapes between the rigid and aeroelastic optimizations is provided in figure 14.

Table 5: Optimization results of aeroelastic MDO wing

	C_L	C_D	C_{M_x}	C_{M_y}	$V(\mathrm{m}^2)$	$\Delta z_{\mathrm{struc}}(\mathrm{m})$	ΔC_D
Initial	0.4	0.0177	0.143	-0.382	241.0	6.18	-
4 modes	0.4	0.0126	0.184	-0.436	241.0	9.39	**-28.8%**
6 modes	0.4	0.0122	0.187	-0.447	241.0	9.78	**-31.1%**
8 modes	0.4	0.0121	0.187	-0.450	241.0	9.71	**-31.6%**

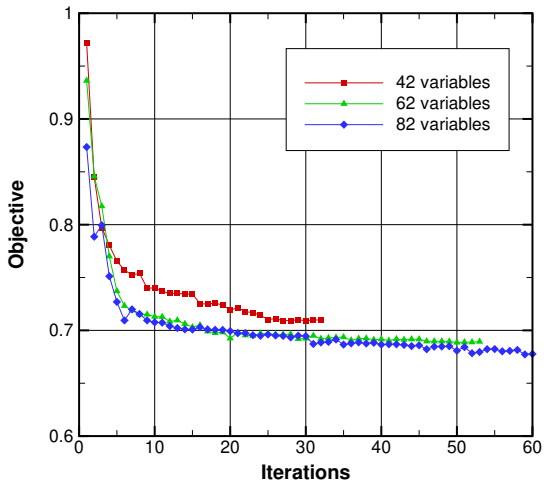

Figure 12: Optimizer convergence for aeroelastic MDO wing

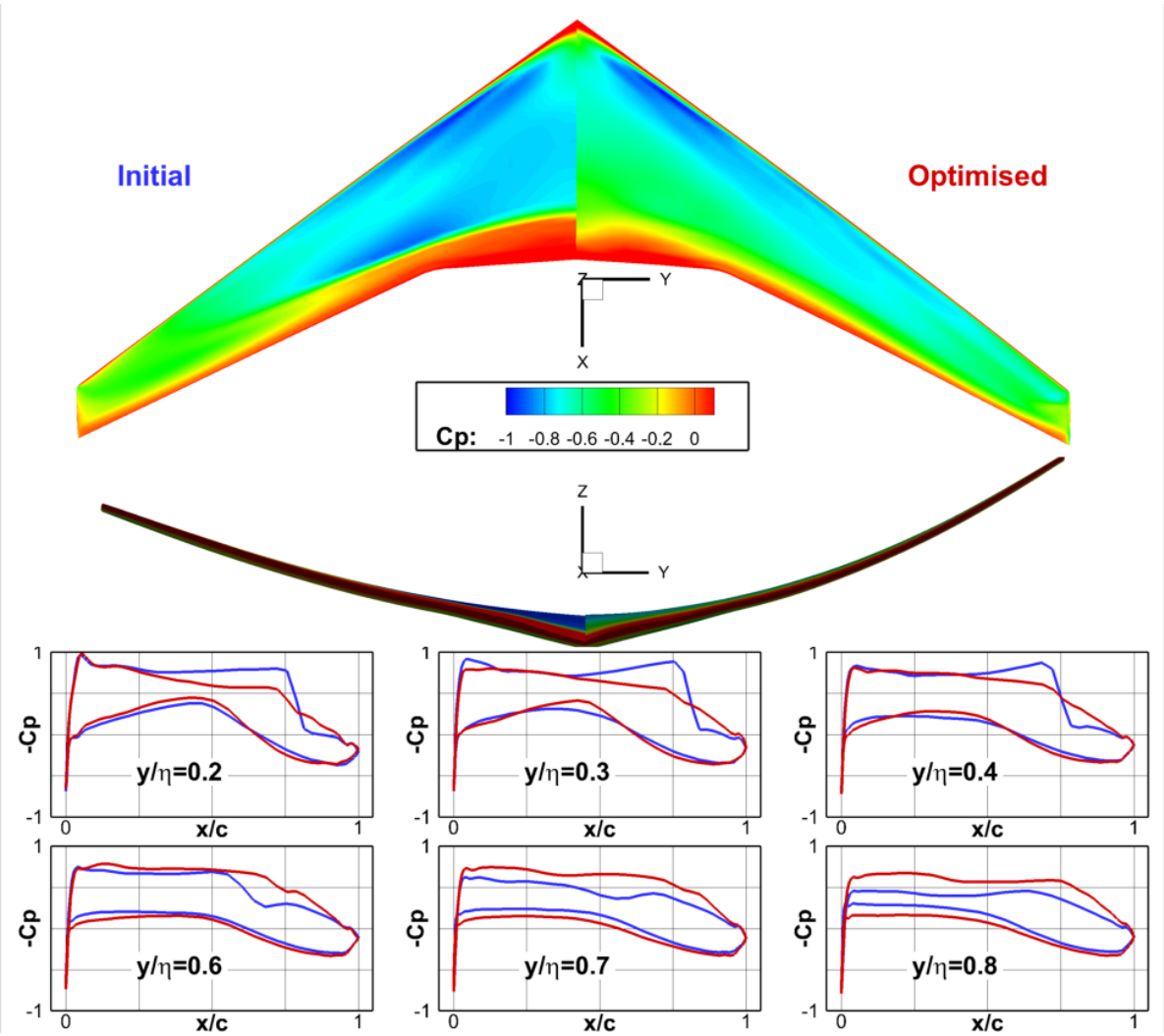

Figure 13: Surface C_P of initial and optimised wing shapes for 8 modes case

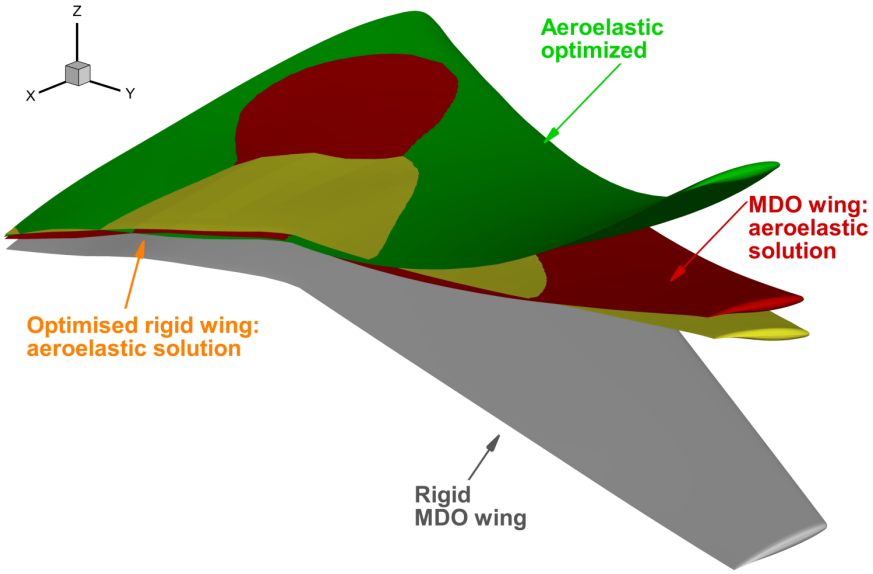

Figure 14: Comparison of rigid and aeroelastic wing shapes

VII. Conclusions

Efficient multi-disciplinary optimization is presented for aero-structural wing optimization using efficient low-dimensional modal design variables. While much aero-structural optimization work to date has considered high-fidelity, many-variable problems, little work has considered the possibility of reducing the dimensionality of the problem. As such, the authors have previously presented an efficient method for determining aerofoil deformations via singular value decomposition. The resulting design variables are geometrically orthogonal resulting in a well-conditioned design space. Hence, in this paper, these are being applied to multi-disciplinary optimization. This work considers these for fixed planform drag minimization of a flexible transonic wing.

The compact aerofoil design variables are applied sectionally for inviscid drag minimization subject to lift and internal volume constraints. The MDO wing has been considered in three different optimization settings, with dimensionality studies also presented. Shock-free solutions were demonstrated for the rigid wing, indicating suitability of the aerofoil modes for sectional-based wing optimization. However, it was demonstrated that a wing designed in rigid shape had poor performance when loaded in flight shape. Hence, the optimization framework was applied the the aeroelastic wing to produce shock-free solutions. The resulting shapes had a much increased tip deflection. The orthogonality behaviour of the modes is preserved through to the optimization and lead to monotonic improvement in objective with increase in dimensionality.

References

[1]Martins, J. R. R. A. and Lambe, A. B., "Multidisciplinary Design Optimization: A Survey of Architectures," *AIAA Journal*, Vol. 51, No. 9, 2013, pp. 2049–2075.
doi:10.2514/1.J051895.

[2]Hicks, R. M. and Henne, P. A., "Wing Design by Numerical Optimization," *Journal of Aircraft*, Vol. 15, No. 7, 1978, pp. 407–412.
doi:10.2514/6.1977-1247.

[3]Qin, N., Vavalle, A., Le Moigne, A., Laban, M., Hackett, K., and Weinerfelt, P., "Aerodynamic Considerations of Blended Wing Body Aircraft," *Progress in Aerospace Sciences*, Vol. 40, No. 6, 2004, pp. 321–343.
doi:10.1016/j.paerosci.2004.08.001.

[4]Allen, C. B. and Rendall, T. C. S., "Computational-Fluid-Dynamics-Based Optimisation of Hovering Rotors Using Radial Basis Functions for Shape Parameterisation and Mesh Deformation," *Optimization and Engineering*, Vol. 14, 2013, pp. 97–118.
doi:10.1007/s11081-011-9179-6.

[5]Poole, D. J., Allen, C. B., and Rendall, T. C. S., "High-fidelity aerodynamic shape optimization using efficient orthogonal modal design variables with a constrained global optimizer," *Computers & Fluids*, Vol. 143, 2017, pp. 1–15.
doi:10.1016/j.compfluid.2016.11.002.

[6]Poole, D. J., Allen, C. B., and Rendall, T. C. S., "Global Optimization of Wing Aerodynamic Optimization Case Exhibiting Multimodality," *Journal of Aircraft*, Vol. 55, No. 4, 2018, pp. 1576–1591.
doi:10.2514/1.C034718.

[7]Geuzaine, P., Brown, G., Harris, C., and Farhat, C., "Aeroelastic Dynamic Analysis of a Full F-16 Configuration for Various Flight Conditions," *AIAA Journal*, Vol. 41, No. 3, 2003, pp. 363–371.
doi:10.2514/2.1975.

[8]Taylor, N. V., Allen, C. B., Gaitonde, A., and Jones, D. P., "A structure-coupled CFD method for time-marching flutter analysis," *The Aeronautical Journal*, Vol. 108, No. 1086, 2004, pp. 389–401.
doi:10.1017/S0001924000000208.

[9]Woodgate, M. A., Badcock, K. J., Rampurawala, A. M., Richards, B. E., Nardini, D., and deC Henshaw, M. J., "Aeroelastic calculations for the Hawk aircraft using the Euler equations," *Journal of Aircraft*, Vol. 42, No. 4, 2005, pp. 1005–1011.
doi:10.2514/1.5608.

[10]Michler, C., Hulshoff, S. J., van Brummelen, E. H., and de Borst, R., "A monolithic approach to fluid-structure interaction," *Computers & Fluids*, Vol. 33, No. 5-6, 2004, pp. 839–848.
doi:10.1016/j.compfluid.2003.06.006.

[11]Hübner, B., Walhorn, E., and Dinkler, D., "A monolithic approach to fluidstructure interaction using spacetime finite elements," *Computer Methods in Applied Mechanics and Engineering*, Vol. 193, No. 23-26, 2004, pp. 2087–2104.
doi:10.1016/j.cma.2004.01.024.

[12]Keye, S. and Mavriplis, D., "Summary of Data from the Sixth AIAA CFD Drag Prediction Workshop: Case 5 (Coupled Aero-Structural Simulation)," *55th AIAA Aerospace Sciences Meeting*, Grapevine, Texas, 2017, AIAA Paper 2017-1207.
doi:10.2514/6.2017-1207.

[13]Rendall, T. C. S. and Allen, C. B., "Unified Fluid-Structure Interpolation and Mesh Motion Using Radial Basis Functions," *International Journal for Numerical Methods in Engineering*, Vol. 74, No. 10, 2008, pp. 1519–1559.
doi:10.1002/nme.2219.

[14]Zhang, Z. J., Khosravi, S., and Zingg, D. W., "High-fidelity aerostructural optimization with integrated geometry parameterization and mesh movement," *Structural and Multidisciplinary Optimization*, Vol. 55, 2017, pp. 1217–1235.
doi:10.1007/s00158-016-1562-7.

[15]Sobieszczanski-Sobieski, J. and Haftka, R. T., "Multidisciplinary aerospace design optimization: survey of recent developments," *Structural Optimization*, Vol. 14, No. 1, 1997, pp. 1–23.
doi:10.1007/BF01197554.

[16]Jameson, A., "Aerodynamic design via control theory," *Journal of Scientific Computing*, Vol. 3, No. 3, 1988, pp. 233–260.
doi:10.1007/BF01061285.

[17]Maute, K., Nikbay, M., and Farhat, C., "Coupled Analytical Sensitivity Analysis and Optimization of Three-Dimensional Nonlinear Aeroelastic Systems," *AIAA Journal*, Vol. 39, No. 11, 2001, pp. 2051–2061.
doi:10.2514/2.1227.

[18]Kenway, G. K. W., Kennedy, G. J., and Martins, J. R. R. A., "Scalable Parallel Approach for High-Fidelity Steady-State Aeroelastic Analysis and Adjoint Derivative Computations," *AIAA Journal*, Vol. 52, No. 5, 2014, pp. 935–951.
doi:10.2514/1.J052255.

[19]Mavriplis, D., Fabiano, E., and Anderson, E., "Recent Advances in High-Fidelity Multidisciplinary Adjoint-Based Optimization with the NSU3D Flow Solver," *55th AIAA Aerospace Sciences Meeting*, Grapevine, Texas, 2017, AIAA Paper 2017-1669.
doi:10.2514/6.2017-1669.

[20]Toal, D. J. J., Bressloff, N. W., Keane, A. J., and Holden, C. M. E., "Geometric Filtration Using Proper Orthogonal Decomposition for Aerodynamic Design Optimization," *AIAA Journal*, Vol. 48, No. 5, 2010, pp. 916–928.
doi:10.2514/1.41420.

[21]Ghoman, S. S., Sarhaddi, D., Chen, P. C., Wang, Z., and Kapania, R. K., "A Hybird Optimization Strategy Using Design-Space Evolution and POD-based Order Reduction," *12th AIAA Aviation Technology, Integration and Operations (ATIO) Conference and 14th AIAA/ISSMO Multidisciplinary Analysis Optimization Conference*, Indianapolis, Indiana, 2012, AIAA Paper 2012-5631.
doi:10.2514/6.2012-5631.

[22]Poole, D. J., Allen, C. B., and Rendall, T. C. S., "Metric-Based Mathematical Derivation of Efficient Airfoil Design Variables," *AIAA Journal*, Vol. 53, No. 5, 2015, pp. 1349–1361.
doi:10.2514/1.J053427.

[23]Allen, C. B., Poole, D. J., and Rendall, T. C. S., "Wing aerodynamic optimization using efficient mathematically-extracted modal design variables," *Optimization and Engineering*, Vol. 19, No. 2, 2018, pp. 453–477.
doi:10.1007/s11081-018-9376-7.

[24]Masters, D. A., Taylor, N. J., Rendall, T. C. S., Allen, C. B., and Poole, D. J., "Geometric Comparison of Aerofoil Shape Parameterization Methods," *AIAA Journal*, Vol. 55, No. 5, 2017, pp. 1575–1589.
doi:10.2514/1.J054943.

[25]Poole, D. J., Allen, C. B., and Rendall, T. C. S., "Efficient Aero-Structural Wing Optimization Using Compact Aerofoil Decomposition," *AIAA Scitech 2019 Forum*, San Diego, California, 2019, AIAA Paper 2019-1701.
doi:10.2514/6.2019-1701.

[26]Eckart, C. and Young, G., "The Approximation of One Matrix by Another of Lower Rank," *Psychometrika*, Vol. 1, No. 3, 1936, pp. 211–218.
doi:10.1007/BF02288367.

[27]Wendland, H., *Scattered Data Approximation*, Cambridge University Press, 1st ed., 2005.

[28]Poole, D. J., Allen, C. B., and Rendall, T. C. S., "Optimal Domain Element Shapes for Free-Form Aerodynamic Shape Control," *53rd AIAA Aerospace Sciences Meeting*, Kissimmee, Florida, 2015, AIAA Paper 2015-0762.
doi:10.2514/6.2015-0762.

[29]Allen, C. B., "Multigrid Convergence of Inviscid Fixed- and Rotary-Wing Flows," *International Journal for Numerical Methods in Fluids*, Vol. 39, No. 2, 2002, pp. 121–140.
doi:10.1002/fld.282.

[30]Allen, C. B., "Parallel simulation of unsteady hovering rotor wakes," *International Journal for Numerical Methods in Engineering*, Vol. 68, No. 6, 2006, pp. 632–649.
doi:10.1002/nme.1723.

[31]Jameson, A., Schmidt, W., and Turkel, E., "Numerical solution of the Euler equations by finite volume methods using Runge Kutta time stepping schemes," *14th Fluid and Plasma Dynamics Conference*, Palo Alto, California, 1981, AIAA Paper 1981-1259.
doi:10.2514/6.1981-1259.

[32]Allen, C. B., "Multigrid Acceleration of an Upwind Euler Method for Hovering Rotor Flows," *The Aeronautical Journal*, Vol. 105, No. 1051, 2001, pp. 517–524.
doi:10.1017/S0001924000017954.

[33]Rendall, T. C. S. and Allen, C. B., "Reduced Surface Point Selection Options Efficient Mesh Deformation Using Radial Basis Functions," *Journal of Computational Physics*, Vol. 229, No. 8, 2010, pp. 2810–2820.
doi:10.1016/j.jcp.2009.12.006.

[34]Newmark, N. M., "A Method of Computation for Structural Dynamics," *Journal of the Engineering Mechanics Division*, Vol. 85, No. 3, 1959, pp. 67–94.

[35]Allwright, S., "Reference aircraft performance and primary sensitivities," Tech. rep., 1997, Technical report D.3.12.R, MDO/TR/BAE/SA970530/1.

[36]Haase, D., Selmin, V., and Winzell, B., *Progress in Computational Flow-Structure Interaction*, Springer, chap. Notes on Numerical Fluid Mechanics and Multidisciplinary design, 2002.

[37]Allen, C. B., "Towards Automatic Structured Multiblock Mesh Generation using Improved Transfinite Interpolation," *International Journal for Numerical Methods in Engineering*, Vol. 74, No. 5, 2008, pp. 697–733.
doi:10.1002/nme.2170.

[38]Yu, Y., Lyu, Z., Xu, Z., and Martins, J. R. R. A., "On the influence of optimization algorithm and initial design on wing aerodynamic shape optimization," *Aerospace Science and Technology*, Vol. 75, 2018, pp. 183–199.
doi:10.1016/j.ast.2018.01.016.

[39]Zhou, J. L., Tits, A. L., and Lawrence, C. T., "Users Guide for FSQP Version 3.7 : A Fortran Code for Solving Optimization Programs, Possibly Minimax, with General Inequality Constraints and Linear Equality Constraints, Generating Feasible Iterates," Tech. rep., Institute for Systems Research, University of Maryland, 1997, SRC-TR-92-107r5.

[40]Mayne, D. Q. and Polack, E., "A superlinearly convergent algorithm for constrained optimization problems," *Mathematical Programming Studies*, Vol. 4, 1982, pp. 45–61.
doi:10.1007/BFb0120947.

[41]Grippo, L., Lampariello, F., and Lucidi, S., "A Nonmonotone Line Search Technique for Newton's Method," *SIAM Journal on Numerical Analysis*, Vol. 23, No. 4, 1986, pp. 707–716.
doi:10.1137/0723046.

[42]Panier, E. R. and Tits, A. L., "Avoiding the Maratos Effect by Means of a Nonmonotone Line Search I. General Constrained Problems," *SIAM Journal on Numerical Analysis*, Vol. 28, No. 4, 1991, pp. 1183–1195.
doi:10.1137/0728063.

[43]Bonnans, J. F., Panier, E. R., Tits, A. L., and Zhou, J. L., "Avoiding the Maratos Effect by Means of a Nonmonotone Line Search II. Inequality Constrained Problems–Feasible Iterates," *SIAM Journal on Numerical Analysis*, Vol. 29, No. 4, 1992, pp. 1187–1202.
doi:10.1137/0729072.

[44]Morris, A. M., Allen, C. B., and Rendall, T. C. S., "CFD-based Optimization of Aerofoils Using Radial Basis Functions for Domain Element Parameterization and Mesh Deformation," *International Journal for Numerical Methods in Fluids*, Vol. 58, No. 8, 2008, pp. 827–860.
doi:10.1002/fld.1769.

[45]Poole, D. J., Allen, C. B., and Rendall, T. C. S., "Comparison of Point Design and Range-Based Objectives for Transonic Aerofoil Optimization," *AIAA Journal*, Vol. 56, No. 8, 2018, pp. 3240–3256.
doi:10.2514/1.J056627.